communications physics

Article

https://doi.org/10.1038/s42005-024-01924-y

Long-range quantum tunneling via matter waves

Check for updates

Yuan-Xing Yang[1,2], Si-Yuan Bai[1,2] & Jun-Hong An[1,2]

Quantum tunneling is a quantum phenomenon in which a microscopic object crosses through a potential barrier even if its energy cannot overcome the barrier. A general belief is that tunneling occurs only when the barrier width is comparable to, or smaller than the de Broglie's wavelength of the object. Here, we study the tunneling of an ultracold atom among N far-separated trapping potentials in a state-selective optical lattice and present a mechanism to realize long-range tunneling. We find that, mediated by the propagating matter wave emitted from the atom, coherent tunneling of the atom to the remote lattices occurs as long as bound states are present in the energy spectrum of the system formed by the atom and its matter-wave. Going beyond the Markovian approximation, and breaking through the conventional distance constraint, our result opens another avenue to realizing tunneling and gives a guideline for developing tunneling devices.

As one of the weirdest effects in the microscopic world, quantum tunneling is a phenomenon consisting of a subatomic particle passing through a potential barrier with a potential energy greater than the energy of the particle[1–8]. It explains various radioactive decay of nuclei and how two nuclei overcome their mutual repulsion and fuse to generate huge energies[9,10]. Quantum tunneling at metallic surfaces is the physical principle behind the operation of the scanning tunneling microscope[11–13]. It also lays a foundation for nanotechnologies, such as the tunnel diode[14] and resonant tunneling[15], and some interdisciplinary sciences including quantum biology[16–18] and quantum chemistry[19,20]. As a ubiquitous behavior of microscopic matters, such as electron[21], proton[22], nucleon[9], photon[23,24], and superconducting Cooper pairs[25], quantum tunneling has been observed in many experiments[20,26–31].

In parallel with its successful applications, the question of how long a particle takes to tunnel through a barrier has remained contentious since the early days of quantum mechanics[1–8]. The progress in ultracold-atom physics and attosecond science makes the direct measurement of the tunneling time possible[32–38]. There is consensus on the fact that quantum tunneling is a consequence of the wave-particle duality and is more likely to occur when the width of the barrier is comparable to or smaller than the de Broglie wavelength of the particle. With the increase of the width of barriers, the tunneling rate experiences an exponential decrease[39,40]. Recently, how to realize long-range tunneling has attracted much attention. For this purpose, the second-order quantum tunneling assisted by photons in the many-body lattice system[41,42], the virtual occupation of an intermediate site in the quantum-dot system[43], and the molecular bridge in the chemical reaction paradigm[44,45] have been proposed. Higher-order resonant tunneling achieved by the interplay between the atomic interactions and the tilted force of the lattice can also realize long-range tunneling up to five lattice sites[46,47]. The chaos in a periodically driven lattice system assists the long-range tunneling too[48]. However, a common necessity of the above works is the nearest-neighbor hopping of the particle, which is equal to the overlap integral of the wave functions in the two sites. It indicates that they still do not essentially go beyond the distance constraint of quantum tunneling.

Inspired by the experimental simulation of the atomic spontaneous emission by the matter-wave of an ultracold atom in a state-selective optical lattice, which is dubbed "quantum optics without photons"[49–51], we propose a scheme to realize long-range tunneling of the atom among the lattice sites. The separation between the lattice sites is so large that the spatial wave functions of the internal ground-state atom confined in the sites have a physically negligible overlap and thus direct tunneling cannot occur. By applying a laser, the atom jumps to the excited state and is converted into a propagating matter-wave. Mediated by this matter wave, long-range tunneling among the lattice sites occurs. It is interesting to find that such tunneling sensitively depends on the features of the energy spectrum of the total system formed by the laser-controlled atom and its matter-wave. As long as bound states out of the continuum (BOCs) or in the continuum (BICs) are present in the energy spectrum, a dynamically periodic tunneling, with frequencies equal to the differences of the energies of the bound states divided by $\hbar$, occurs among the lattice sites. This periodicity makes the tunneling time in our system well-defined and experimentally measurable. Breaking through the conventional distance constraint on quantum tunneling, our result is beneficial to designing quantum tunneling devices.

[1]School of Physical Science and Technology & Lanzhou Center for Theoretical Physics, Lanzhou University, Lanzhou, China. [2]Key Laboratory of Quantum Theory and Applications of MoE & Key Laboratory of Theoretical Physics of Gansu Province, Lanzhou University, Lanzhou, China. e-mail: anjhong@lzu.edu.cn

Results and discussion

Model

The ultracold-atom system offers us an ideal platform to simulate quantum optics and many-body physics[52–58]. Inspired by the experiments of the emission of atomic matter waves[49–51], we investigate the tunneling dynamics of an ultracold atom in an optical lattice. Having two hyperfine states $|a\rangle$ and $|b\rangle$ and a mass m, the atom is confined in a state-selective optical lattice with N unoccupied sites[58]. The lattice is embedded in an isolated tube, see Fig. 1. When the atomic internal state is $|a\rangle$, it is trapped in the spatial ground state $\Phi_a(z) = (\sqrt{\pi}\bar{z})^{-1/2}\exp[-z^2/(2\bar{z}^2)]$, with an eigenenergy $\tilde{\omega}/2$ and $\bar{z} = \sqrt{\hbar/(m\tilde{\omega})}$, by the lattice potential $V(z) = m\tilde{\omega}^2 z^2/2$. Thus, the movement of the $|a\rangle$-state atom to other lattice sites is classically forbidden. Introducing an operator $\hat{\sigma}_j \equiv |0\rangle_j\langle 1|$, with $|0\rangle_j$ and $|1\rangle_j$ denoting the unoccupied and occupied states of the atom in the j th lattice site, we rewrite the Hamiltonian of the $|a\rangle$-state atom $\hat{H}_a = \sum_{j=1}^{N}\hbar(\omega_a + \tilde{\omega}/2)\hat{\sigma}_j^\dagger\hat{\sigma}_j$ with ω_a being the bare frequency of $|a\rangle$. On the contrary, when the atom is in the excited state $|b\rangle$ with a bare frequency ω_b, it is set free from the site and propagates as a matter wave $\Phi_{b,k}(z) = e^{ikz}/\sqrt{L}$ along the tube, with L being the tube length and $k = 2\pi n/L$ ($n \in \mathbb{Z}$). Without feeling the optical lattice, the $|b\rangle$-state atom also has no chance to move to other lattice sites. The Hamiltonian of the $|b\rangle$-state atom is $\hat{H}_b = \sum_k\hbar[\omega_b + \hbar k^2/(2m)]\hat{b}_k^\dagger\hat{b}_k$, where $\hat{b}_k$ is the annihilation operator of the k th mode of the emitted matter-wave quanta. The states $|a\rangle$ and $|b\rangle$ are coupled by a microwave field such that the atom performs the Rabi oscillation described by $\hat{H}_{ab} = \frac{\hbar\Omega}{2}\sum_{j=1}^{N}\sum_k(\gamma_{jk}e^{i\omega_L t}\hat{\sigma}_j^\dagger\hat{b}_k + \text{h.c.})$, where Ω and ω_L are the strength and the frequency of the driving field, and $\gamma_{jk} = \int dz\Phi_a(z - z_j)\Phi_{b,k}^*(z)$ is the Franck-Condon overlap between the trapped wave function at the j th site and the k th mode of the matter wave. The lattice sites are assumed to be so far separated that the overlap of the wave functions of the atom in different sites is much smaller than $|\gamma_{jk}|$ and thus the direct tunneling among them is negligible. This endows a substantial difference in our scheme from the ones in refs. 41–48, where the nearest-neighbor hopping is necessary. In a rotating frame $\hat{H}_0 = \sum_j\hbar(\omega_b - \omega_L)\hat{\sigma}_j^\dagger\hat{\sigma}_j + \sum_k\hbar\omega_b\hat{b}_k^\dagger\hat{b}_k$, the total Hamiltonian becomes[59]

$$\frac{\hat{H}}{\hbar} = \omega_0\sum_{j=1}^{N}\hat{\sigma}_j^\dagger\hat{\sigma}_j + \sum_k[\omega_k\hat{b}_k^\dagger\hat{b}_k + \sum_{j=1}^{N}(g_{jk}\hat{\sigma}_j^\dagger\hat{b}_k + \text{h.c.})], \tag{1}$$

where $\omega_0 = \omega_a + \frac{\tilde{\omega}}{2} - \omega_b + \omega_L$, $\omega_k = \frac{\hbar k^2}{2m}$, and $g_{jk} = \frac{\Omega\gamma_{jk}}{2}$. Having a rotating-wave approximate form, Eq. (1) guarantees the number of the atom always to be one. It rules out the nonphysical scenarios that a propagating $|b\rangle$-state atom and a trapped $|a\rangle$-state atom are created and annihilated simultaneously, which, respectively, are described by $\hat{\sigma}_j^\dagger\hat{b}_k^\dagger$ and $\hat{\sigma}_j\hat{b}_k$. The single-site case of Eq. (1) has been experimentally realized in refs. 49,50. It is noted that Eq. (1) takes the same form as the Tavis–Cummings model with a multimode boson field[60]. Here, the N sites of the optical lattice play the role of N identical two-level systems, each being separately coupled with the field.

Tunneling dynamics

Considering the atom is initially in the first lattice site, we have $|\Psi(0)\rangle = |a_1, \{0_k\}\rangle$. Its evolved state can be expanded as $|\Psi(t)\rangle = \sum_{j=1}^{N}c_j(t)|a_j, \{0_k\}\rangle + \sum_k d_k(t)|b, 1_k\rangle$, where $|a_j, \{0_k\}\rangle$ denotes that the atom in the state $|a\rangle$ is confined in the j th lattice site and no wave-matter quanta is triggered in the isolated tube and $|b, 1_k\rangle$ denotes that the atom in the state $|b\rangle$ propagates in the isolated tube as a matter-wave quanta in the k th mode. From the Schrödinger equation, we derive the equation of motion satisfied by the column vector $\mathbf{c}(t) = (c_1(t)\cdots c_N(t))^{\mathrm{T}}$ formed by the probability amplitudes of the atom in the N sites as

$$\dot{\mathbf{c}}(t) + i\omega_0\mathbf{c}(t) + \int_0^t d\tau\mathbf{f}(t-\tau)\mathbf{c}(\tau) = 0. \tag{2}$$

Here $\mathbf{f}(t-\tau) = \int_0^\infty d\omega e^{-i\omega(t-\tau)}\mathbf{J}(\omega)$ is a N-by-N correlation-function matrix of the matter wave and the element of the matrix $\mathbf{J}(\omega)$ is defined as $J_{jl}(\omega) = \sum_k g_{jk}^* g_{lk}\delta(\omega - \omega_k)$ characterizing the correlated spectral density of the atom in the j th and l th lattice sites. Such a correlation indicates that, although direct tunneling of the atom among different lattice sites is absent, the mediated tunneling via the $|b\rangle$-state matter wave is triggered by the Rabi oscillation. One can readily derive

$$J_{jl}(\omega) = J_{|j-l|}(\omega) = \frac{\Omega^2 e^{\frac{-2\omega}{\tilde{\omega}}}}{\sqrt{8\pi\tilde{\omega}\omega}}\cos\left[\left(\frac{2\omega}{\tilde{\omega}}\right)^{\frac{1}{2}}\frac{z_j - z_l}{\bar{z}}\right]. \tag{3}$$

Reflecting the memory effect, the convolution in Eq. (2) renders the tunneling dynamics non-Markovian. Its dominant role in the dynamics has been observed[49,51].

In the special case of the small-Ω limit, we can make the Markovian approximation to Eq. (2) by replacing $\mathbf{c}(\tau)$ with $\mathbf{c}(t)$ and extending the upper limit of the time integral to infinity[61,62]. This approximation is also applicable when the spectral density reduces to a constant. The obtained solution is

$$\mathbf{c}_{\mathrm{MA}}(t) = \exp[-(\boldsymbol{\kappa} + i\omega_0 + i\boldsymbol{\Delta})t]\mathbf{c}(0), \tag{4}$$

where $\boldsymbol{\kappa} = \pi\mathbf{J}(\omega_0)$ and $\boldsymbol{\Delta} = \mathcal{P}\int\frac{\mathbf{J}(\omega)d\omega}{\omega_0 - \omega}$, with $\mathcal{P}$ being the Cauchy's principal value. We see that $|\mathbf{c}_{\mathrm{MA}}(t)|^2$ exponentially decays to zero due to the positivity of $\boldsymbol{\kappa}$. Thus, the atom asymptotically relaxes to the tube as a matter wave and no tunneling to other lattice sites occurs in the long-time condition of the Markovian dynamics. An exception occurs when $\omega_0 < 0$, where $\boldsymbol{\kappa} = 0$ but $\boldsymbol{\Delta} \neq 0$, and thus a lossless tunneling can happen via exchanging the virtual matter waves[63].

The strong driving invalidates the Markovian approximation. In the general non-Markovian case, Eq. (2) can only be solved numerically. However, its asymptotic form is solvable by the Laplace transform method. It converts Eq. (2) into $[s + i\omega_0 + \tilde{\mathbf{f}}(s)]\tilde{\mathbf{c}}(s) = \mathbf{c}(0)$, where $\tilde{\mathbf{f}}(s) = \int_0^\infty d\omega\frac{\mathbf{J}(\omega)}{s+i\omega}$. Using the Jordan decomposition $\mathbf{D}(s) = \mathbf{V}_s^{-1}\tilde{\mathbf{f}}(s)\mathbf{V}_s = \mathrm{diag}[D_1(s), \cdots, D_N(s)]$, we obtain $\tilde{\mathbf{c}}(s) = \mathbf{V}_s\left[s + i\omega_0 + \mathbf{D}(s)\right]^{-1}\mathbf{V}_s^{-1}\mathbf{c}(0)$. $\mathbf{c}(t)$ is calculated by making the inverse Laplace transform $\tilde{\mathbf{c}}(s)$, which needs

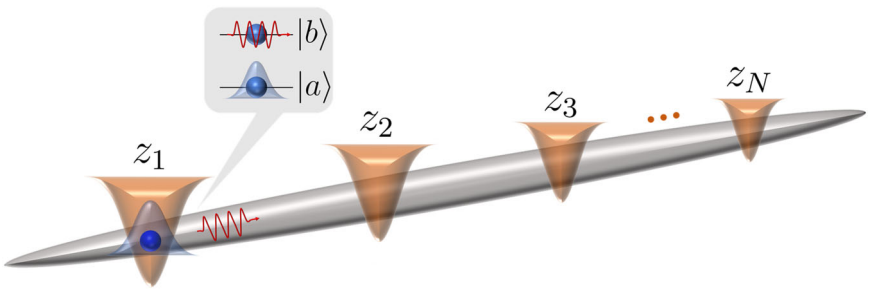

Fig. 1 | Scheme of the system. An ultracold atom is confined in a state-selective optical lattice with different sites labeled by z_j ($j = 1, \cdots, N$) wrapped by an isolated tube. When it is in the ground state $|a\rangle$, the atom is trapped in the sites. When it is in the excited state $|b\rangle$, it propagates in the tube as a matter wave. The two states are coupled by a laser. The separation between the sites is so large that atomic direct tunneling among the sites is impossible.

finding the poles of $\tilde{\mathbf{c}}(s)$ from $(\varpi = is)$

$$Y_j(\varpi) \equiv \omega_0 - iD_j(-i\varpi) = \varpi,\ (j = 1, \cdots, N). \tag{5}$$

It is found that the root ϖ multiplied by $\hbar$ is just the eigenenergy of Eq. (1). It indicates that the atomic tunneling dynamics described by $\mathbf{c}(t)$ is intrinsically determined by the features of the energy spectrum of the total system formed by the confined atom and its propagating matter-wave. We find that Eq. (5) has three types of roots. First, $Y_j(\varpi)$ is ill-defined in the region of $\varpi > 0$ due to the poles in $D_j(-i\varpi)$, and thus Eq. (5) has an infinite number of roots, which form a continuous energy band. Second, because $Y_j(\varpi)$ is a decreasing function in the region out of the continuum, i.e., $\varpi < 0$, Eq. (5) has an isolated root $\varpi_j^{\rm boc}$ provided $Y_j(0) < 0$. The eigenstate corresponding to $\hbar\varpi_j^{\rm boc}$ is called a BOC. Third, a removable singularity $\varpi_j^{\rm bic}$ exists for $D_j(-i\varpi)$ when $\omega_0 = \varpi_j^{\rm bic} + iD_j(-i\varpi_j^{\rm bic})$ also fulfills Eq. (5). The eigenstate corresponding to $\hbar\varpi_j^{\rm bic}$ is called a BIC. The formation of the BOC and BIC has profound consequences on the non-Markovian dynamics[64–68]. According to the Cauchy's residue theorem and contour integration, we have[69]

$$\mathbf{c}(t) = \mathbf{Z}(t) + \int_0^\infty \frac{d\varpi}{2\pi}[\tilde{\mathbf{c}}(0^+ - i\varpi) - \tilde{\mathbf{c}}(0^- - i\varpi)]e^{-i\varpi t}, \tag{6}$$

where $\mathbf{Z}(t) = \sum_{\alpha={\rm bic,boc}}\sum_{j=1}^{N}{\rm Res}[\tilde{\mathbf{c}}(-i\varpi_j^\alpha)]e^{-i\varpi_j^\alpha t}$, with ${\rm Res}\,[\tilde{\mathbf{c}}(-i\varpi_j^\alpha)]$ is the residue contributed by the j th bound state obtained from $Y_j(\varpi) = \varpi$, and the second term comes from the continuous energy band. Containing an infinite number of superposition components oscillating with time in continuously changing frequencies ϖ, the second term tends to zero in the long-time limit due to the out-of-phase interference. Thus, if the bound state is absent, then $\lim_{t\to\infty}\mathbf{c}(t) = \mathbf{0}$ characterizes a complete relaxation of the atom in the isolated tube, while if the bound states are formed, then $\lim_{t\to\infty}\mathbf{c}(t) = \mathbf{Z}(t)$ implies a stable tunneling of the atom among the lattice sites. The result reveals that we can achieve a persistent matter-wave mediated long-range tunneling of the atom among the optical lattice by manipulating the formation of the bound states even when the lattice sites are so separated that direct tunneling cannot happen. It inspires that, parallel to the rapidly developing electromagnetic-wave-based waveguide QED[70], our matter-wave-based waveguide supplies another realization of the efficient interconnect among well-separated spatial nodes[71]. Note that, besides the real-valued eigenenergies of the BIC and BOC, Eq. (5) also has complex-value eigenvalues. They can be found by analytically extending the function to the second Riemann sheet[72]. These complex-valued eigenenergies contribute unstable oscillations and thus do not survive in the long-time tunneling dynamics.

First, we assume that the lattice has two sites, i.e., $N = 2$. It is easy to derive $D_{1/2}(s) = \tilde{f}_0(s) \pm \tilde{f}_1(s)$ and $\mathbf{V}_s = \begin{pmatrix} 1 & 1 \\ 1 & -1 \end{pmatrix}$. We thus have $\tilde{\mathbf{c}}(s) = \mathbf{M}[s + i\omega_0 + \mathbf{D}(s)]^{-1}\begin{pmatrix} 1 & 1 \end{pmatrix}^{\rm T}$, where $\mathbf{M} = \begin{pmatrix} 1/2 & 1/2 \\ 1/2 & -1/2 \end{pmatrix}$. If the bound states are present, then

$$c_j(\infty) = \sum_{\alpha\in{\rm bic,boc}}\sum_{l=1}^{2} M_{jl}Z_l^\alpha e^{-i\varpi_l^\alpha t}, \tag{7}$$

where $Z_l^\alpha = [1 + \partial_s D_l(s)]^{-1}|_{s\to -i\varpi_l^\alpha}$. The l th BOC is formed when $Y_l(0) < 0$. The divergence of $D_{1/2}(s)$ is removed by the BIC frequency determined $J_0(\omega_{1/2}^{\rm bic}) \pm J_1(\omega_{1/2}^{\rm bic}) = 0$ as

$$\varpi_{1/2}^{\rm bic} = \tilde{\omega}(\bar{z}n_{1/2}\pi/d)^2/2, \tag{8}$$

with $d = |z_1 - z_2|$, n_1 and n_2 being odd and even numbers, under the condition $\omega_0 = \varpi_l^{\rm bic} + iD_l(-i\varpi_l^{\rm bic})$. Equation (7) clearly shows that, in sharp contrast to complete relaxation to the isolated tube as a matter wave under the Markovian approximation in Eq. (4), a stable distribution and a persistently oscillating tunneling of the atom between the two sites occur when one and two bound states are formed, respectively. Such tunneling mediated by the matter wave has not been reported before.

We plot in Fig. 2a the energy spectrum of the system. It is found that two branches of BOCs are present and one BIC is formed at $\omega_0 = 0.18\tilde{\omega}$. The evolution of the modulus of the atomic probability amplitudes in the two lattice sites in Fig. 2b, c shows that the atom completely relaxes into the isolated tube when no bound state is formed in the regime $\omega_0 > 0.25\tilde{\omega}$, which has no difference from the Markovian result in Eq. (4). In the regime $\omega_0 \in (0.058, 0.25)\tilde{\omega}$, one BOC is formed and thus both $|c_1(t)|$ and $|c_2(t)|$ tend to equal constants, see the orange squares in Fig. 2d, e. This corresponds to a stable distribution of the atom in the two lattice sites. An exception occurs when $\omega_0 = 0.18\tilde{\omega}$, where a BIC and a BOC coexist, and thus the atom experiences a lossless oscillation between the two lattice sites in a frequency $|\varpi_1^{\rm boc} - \varpi_2^{\rm bic}|$, see the green rhombuses in Fig. 2d, e. Such a lossless oscillation between the two lattice sites can also occur in a frequency $|\varpi_1^{\rm boc} - \varpi_2^{\rm boc}|$ when two BOCs are present in the regime $\omega_0 < 0.058\tilde{\omega}$, see the blue circles in Fig. 2d, e. The matching of the numerical results with the analytic ones in Eq. (7) for the three typical parameter regimes confirms the dominant role of the bound states in the long-time dynamics. This lossless oscillation characterizes coherent tunneling of the atom between the two sites mediated by the propagating matter-wave. Thus, we achieve long-range coherent tunneling even when the sites are so separated that the spatial wave functions of the atom have a negligible overlap.

Figure 3a shows the energy spectrum of the system in different site separations d. Two branches of BOCs separate the spectrum into two regimes: one BOC when $d \le 5\bar{z}$ and two BOCs when $d > 5\bar{z}$. A BIC is formed at $d = 8.67\bar{z}$ and $17.36\bar{z}$, respectively. The evolution of $|c_j(t)|$ in Fig. 3b, c indicates that $|c_1(t)|$ and $|c_2(t)|$ evolve to an equal constant in the single-BOC regime and experience a lossless oscillation with a common period $T = 2\pi/|\varpi_1^{\rm boc} - \varpi_2^{\rm boc}|$ and a $\pi/2$ phase difference in the two-BOC regime. The latter reveals that the atom coherently goes back and forth between the two sites. With increasing d, $\varpi_1^{\rm boc}$ tends closer and closer to $\varpi_2^{\rm boc}$, and thus the period T for the atom to finish one cyclic tunneling between the two sites becomes longer and longer. At the two distances in the presence of the BIC, $|c_j(t)|$ behaves as a periodic oscillation with three frequencies, i.e., $|\varpi_1^{\rm boc} - \varpi_2^{\rm boc}|$ and $|\varpi_j^{\rm boc} - \varpi^{\rm bic}|$ $(j = 1, 2)$. The phase diagram for forming different numbers of bound states in the d-ω_0 plane is shown in Fig. 3d. The formed zero, one, and two BOCs separate the diagram into three parts. Several discrete curves supporting the formation of the BIC in different n_l are added above the diagram. It gives a global picture of the features of atomic tunneling. If no bound state is present, then the atom relaxes as a matter wave in the tube. If one bound state is formed, then it tends to a stable equal probability distribution in the two sites. If two or three bound states are formed, then the atom periodically and losslessly oscillates between the two sites in frequencies proportional to the eigenenergy difference of any pair of the bound states.

Our result can be generalized to the multiple-site case. When $N = 3$, we have $D_1(s) = \tilde{f}_0 - \tilde{f}_2$, $D_{2/3}(s) = \tilde{f}_0 + \frac{1}{2}(\tilde{f}_2 \mp \tilde{e})$, and $\mathbf{V}_s = \begin{pmatrix} -1 & 1 & 1 \\ 0 & \frac{\tilde{f}_1(\tilde{e}-3\tilde{f}_2)}{\tilde{f}_2\tilde{e}-2\tilde{f}_1^2-\tilde{f}_2^2} & \frac{\tilde{f}_1(\tilde{e}+3\tilde{f}_2)}{\tilde{f}_2\tilde{e}+2\tilde{f}_1^2+\tilde{f}_2^2} \\ 1 & 1 & 1 \end{pmatrix}$, where the argument s of $\tilde{f}_j(s)$ has been omitted for brevity and $\tilde{e} = (8\tilde{f}_1^2 + \tilde{f}_2^2)^{\frac{1}{2}}$. It is obtained that $\tilde{\mathbf{c}}(s) = \mathbf{M}[s + i\omega_0 + \mathbf{D}(s)]^{-1}\begin{pmatrix} 1 & 1 & 1 \end{pmatrix}^{\rm T}$, where $\mathbf{M} = \begin{pmatrix} 1/2 & \frac{1-\tilde{f}_2/\tilde{e}}{4} & \frac{1+\tilde{f}_2/\tilde{e}}{4} \\ 0 & -\tilde{f}_1/\tilde{e} & \tilde{f}_1/\tilde{e} \\ -1/2 & \frac{1-\tilde{f}_2/\tilde{e}}{4} & \frac{1+\tilde{f}_2/\tilde{e}}{4} \end{pmatrix}$. The BIC for $D_1(s)$ is formed at $\varpi_1^{\rm bic} = \tilde{\omega}(\bar{z}n\pi/d)^2/8$, with n being an even number. According to the residue theorem, we have

$$c_j(\infty) = \sum_{\alpha={\rm bic,boc}}\sum_{l=1}^{3}\frac{M_{jl}e^{st}}{1 + \partial_s D_l(s)}\bigg|_{s\to -i\varpi_l^\alpha}. \tag{9}$$

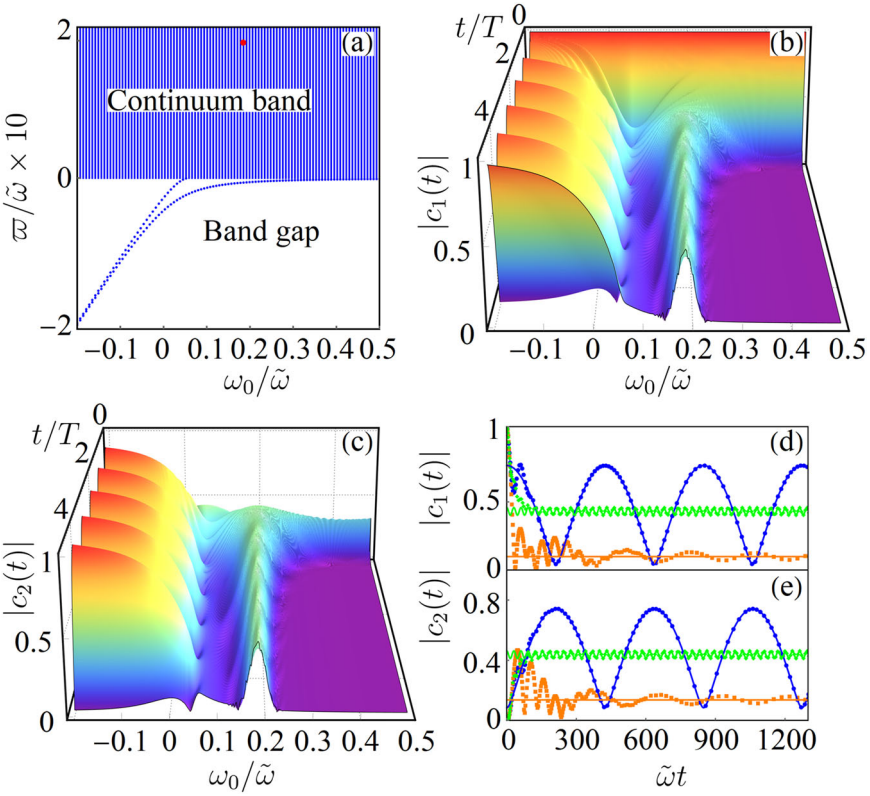

Fig. 2 | Energy spectrum and dynamics for different values of atomic frequency detuning in the case of two lattice sites. a Energy spectrum and evolution of the absolute values of the probability amplitudes (**b**) $|c_1(t)|$ in the first site and (**c**) $|c_2(t)|$ in the second site for different values of atomic frequency detuning ω_0. The red dot in **a** marks the energy of the bound state in the continuum. T in **b** and **c** defined as $2\pi/|\bar{\omega}_1^{\rm boc}-\bar{\omega}_2^{\rm boc/bic}|$ is the oscillation period in the steady state. Evolution of (**d**) $|c_1(t)|$ and (**e**) $|c_2(t)|$ when $\omega_0=-0.02\tilde{\omega}$ (blue dots), $0.06\tilde{\omega}$ (orange squares), and $0.18\tilde{\omega}$ (green rhombuses). Their long-time behaviors evaluated from Eq. (7) are shown by the solid lines in the same colors. We use $d=5\bar{z}$, $\Omega=0.13\tilde{\omega}$, $\bar{z}=0.065$ nm, and $\tilde{\omega}=2\pi\times 40$ kHz.

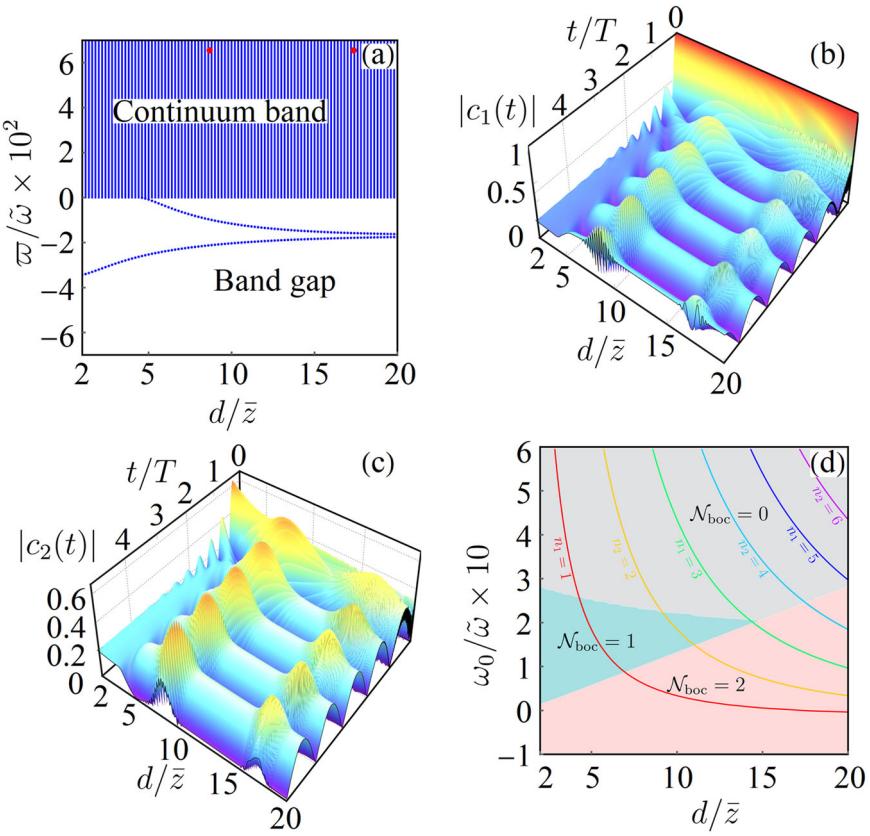

Fig. 3 | Energy spectrum and dynamics for different values of the site separations in the case of two lattice sites. a Energy spectrum and evolution of the absolute values of the probability amplitudes (**b**) $|c_1(t)|$ in the first site and (**c**) $|c_2(t)|$ in the second site for different values of the lattice-site separation d when $\omega_0=0.05\tilde{\omega}$. Red dots in **a** mark the energies of the bound states in the continuum. **d** Phase diagram for forming different numbers of bound states out of the continuum denoted by $\mathcal{N}_{\rm boc}$ in the $d-\omega_0$ plane. The solid lines evaluated from Eq. (8) for different n_l in **c** mark the positions forming the bound states in the continuum. Other parameters are the same as in Fig. 2.

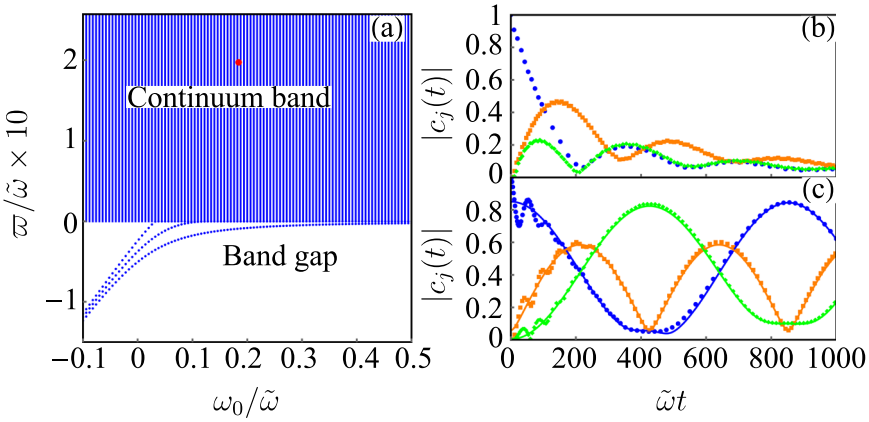

Fig. 4 | Energy spectrum and dynamics for different values of the atomic frequency detuning in the case of three lattice sites. a Energy spectrum and evolution of the absolute values of the probability amplitudes $|c_1(t)|$ (blue dots), $|c_2(t)|$ (orange squares), and $|c_3(t)|$ (green rhombuses) when the atomic frequency detuning $\omega_0 = 0.4\tilde{\omega}$ in **b** and $-0.05\tilde{\omega}$ in **c** for the atom tunneling among three lattice sites. The red dot in **a** marks the energy of the bound state in the continuum. The long-time behaviors evaluated from Eq. (31) are shown by the solid lines in the same colors in **c**. We use $d = 5\bar{z}$ and $\Omega = 0.13\tilde{\omega}$.

The energy spectrum in Fig. 4a shows that three BOCs and one BIC at most are formed. Without the bound state, the atom relaxes as a matter wave in the tube and no occupation in the sites survives, see Fig. 4b. When three BOCs are present, $|c_1(t)|$ and $|c_2(t)|$ tend to a lossless oscillation in three frequencies $|\varpi_i^{\rm boc} - \varpi_j^{\rm boc}|$ $(i, j = 1, 2, 3)$, and $|c_2(t)|$ behaves as an oscillation in a frequency $|\varpi_2^{\rm boc} - \varpi_3^{\rm boc}|$, see Fig. 4c. They match our analytical result (9) and verify the distinguished bound-state role in the tunneling dynamics. The result confirms again that we can realize long-range tunneling among the lattice sites by the mediation of the matter wave.

Conclusions

We have studied the tunneling dynamics of an ultracold atom in a state-selective optical lattice embedded in an isolated tube. A mechanism to realize long-range tunneling of the atom among the lattice sites via the mediation of its propagating matter wave is found. In contrast to one's general belief that tunneling occurs when the atomic wavelength exceeds the width of the confined potential, our result reveals an alternative tunneling by converting the atom into a matter wave. We find that such tunneling can be controlled by engineering the features of the energy spectrum of the system. When zero, one, and more BOCs or BICs are present in the energy spectrum, the tunneling exhibits complete relaxation in the tube, stable distribution, and lossless oscillation among the lattice sites, respectively. The observation of the bound-state effect in the single-lattice-site case[49,51] gives support to realize our scheme. Supplying insightful instruction to realize controllable long-range tunneling, our result is helpful not only to simulating many-body physics with long-range orders[58,73], but also to designing quantum-tunneling[74] and -interconnect[71,75] devices. In parallel to cavity[76,77], circuit[78,79], and waveguide QED systems[80,81], our matter-wave setup supplies a perfect realization of quantum interconnect among different quantum nodes. The matter-wave version is advantageous over the photonic platforms because there is no loss for the matter waves.

Methods

Derivation of dynamical evolution

The initial state of the total system is $|\Psi(0)\rangle = |a_1, \{0_k\}\rangle$. Its evolved state is expanded as $\Psi(t)\rangle = \sum_{j=1}^{N} c_j(t)|a_j, \{0_k\}\rangle + \sum_k d_k(t)|b, 1_k\rangle$. From the Schrödinger equation, we derive

$$i\dot{c}_j(t) = \omega_0 c_j(t) + \sum_k g_{jk} d_k(t), \tag{10}$$

$$i\dot{d}_k(t) = \omega_k d_k(t) + \sum\nolimits_{l=1}^{N} g_{lk}^* c_l(t). \tag{11}$$

Substituting the solution of Eq. (11) $d_k(t) = -i\sum_l \int_0^t d\tau g_{lk}^* e^{-i\omega_k(t-\tau)} c_l(\tau)$ under the initial condition $d_k(0) = 0$ into Eq. (10), we have

$$\dot{c}_j(t) + i\omega_0 c_j(t) + \sum_{l=1}^{N} \int_0^t d\tau f_{jl}(t-\tau) c_l(\tau) = 0, \tag{12}$$

where $f_{jl}(t-\tau) = \int_0^\infty d\omega J_{jl}(\omega) e^{-i\omega(t-\tau)}$ is the correlation function of the matter wave and $J_{jl}(\omega) = \sum_k g_{jk} g_{lk}^* \delta(\omega - \omega_k)$ is the correlated spectral density of the atom between the j th and l th lattice sites. Remembering the form of g_{jk} and γ_{jk} and making the continuum limit of k under $L \gg \bar{z}$, we obtain

$$\begin{aligned} rclJ_{jl}(\omega) &= \frac{\Omega^2\sqrt{\pi}\bar{z}}{2L} \sum_k e^{-\bar{z}^2 k^2 - ik(z_l - z_j)} \delta(\omega - \omega_k) \\ &= \frac{\Omega^2 e^{\frac{-2\omega}{\tilde{\omega}}}}{\sqrt{8\pi\tilde{\omega}\omega}} \cos\left[\left(\frac{2\omega}{\tilde{\omega}}\right)^{\frac{1}{2}} \frac{z_j - z_l}{\bar{z}}\right]. \end{aligned} \tag{13}$$

We see that $J_{11}(\omega) = \cdots = J_{NN}(\omega)$ and $J_{jl}(\omega) = J_{lj}(\omega)$. Thus, J_{jl} satisfies the property $J_{jl}(\omega) = J_{|j-l|}(\omega)$. Equation (12) is rewritten as a column-vector form

$$\dot{\mathbf{c}}(t) + i\omega_0 \mathbf{c}(t) + \int_0^t d\tau \mathbf{f}(t-\tau)\mathbf{c}(\tau) = 0, \tag{14}$$

where $\mathbf{c}(t) = (c_1(t) \cdots c_N(t))^{\rm T}$, $\mathbf{f}(t-\tau) = \int_0^\infty d\omega e^{-i\omega(t-\tau)} \mathbf{J}(\omega)$ is an N-by-N matrix with its elements being the correlation function $f_{jl}(t-\tau)$, and $\mathbf{J}(\omega)$ is an N-by-N matrix with its elements being the correlated spectral density $J_{jl}(\omega)$. Via a Laplace transform $\tilde{\mathbf{c}}(s) \equiv \int_0^\infty e^{-st}\mathbf{c}(t)dt$, Eq. (14) is converted into $[s + i\omega_0 + \tilde{\mathbf{f}}(s)]\tilde{\mathbf{c}}(s) = \mathbf{c}(0)$, where $\tilde{\mathbf{f}}(s) = \int_0^\infty d\omega \frac{\mathbf{J}(\omega)}{s+i\omega}$ is the Laplace transform of $\mathbf{f}(t-\tau)$. Using the Jordan decomposition of $\tilde{\mathbf{f}}(s)$ as

$$\mathbf{D}(s) = \mathbf{V}_s^{-1}\tilde{\mathbf{f}}(s)\mathbf{V}_s = \ {\rm diag}\,[D_1(s), \cdots, D_N(s)], \tag{15}$$

we have

$$\begin{aligned} \tilde{\mathbf{c}}(s) &= \mathbf{V}_s[s + i\omega_0 + \mathbf{D}(s)]^{-1}\mathbf{V}_s^{-1}\mathbf{c}(0) \\ &= \mathbf{M}[s + i\omega_0 + \mathbf{D}(s)]^{-1}\begin{pmatrix}1 & \cdots & 1\end{pmatrix}^{\rm T}. \end{aligned} \tag{16}$$

The inverse Laplace transform reads $\mathbf{c}(t) = \int_{\gamma-i\infty}^{\gamma+i\infty} \frac{e^{st}}{2\pi i}\tilde{\mathbf{c}}(s)$, where γ is chosen such that all the poles are included. According to the contour integration, see Fig. 5, the evaluation of the inverse Laplace transform needs finding the poles of $\tilde{\mathbf{c}}(s)$ from

$$s + i\omega_0 + D_j(s) = 0. \tag{17}$$

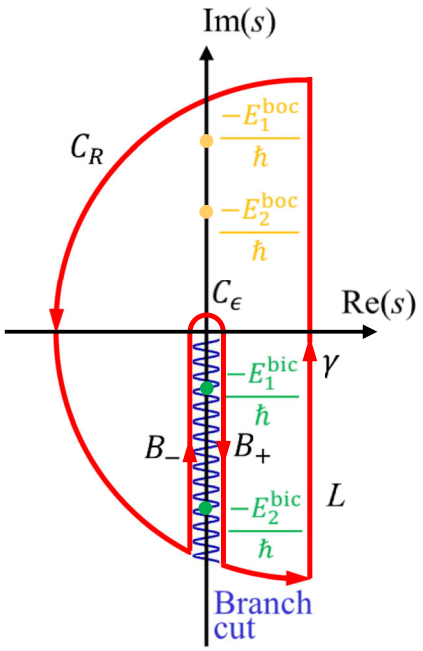

Fig. 5 | Contour integration to evaluate the inverse Laplace transform. Path of the contour integration in the complex plane $\mathrm{Re}(s)+i\mathrm{Im}(s)$ for the calculation of the inverse Laplace transform $\tilde{\mathbf{c}}(s)$. The radii C_R tends to infinity and C_ϵ tends to zero. The continuous poles form a branch cut wrapped by two inverse paths $B_\pm$. The isolated poles form the bound states out of the continuum with eigenenergies E_j^{boc} in the positive-Im(s) axis and the bound states in the continuum with eigenenergies E_j^{bic} in the negative-Im(s) axis.

In general, Eq. (17) has three types of poles determined by $D_j(s)$, see Fig. 5. The first one is a continuum of poles along the negative imaginary axis of the complex plane formed by the real and imaginary parts of s, which forms a branch cut. The second one is several discrete roots formed by the removable singularities of $D_j(s)$ along the negative imaginary axis, which is called the BIC. The third one is the isolated poles along the positive imaginary axis, which is called the BOC.

According to the Cauchy's residue theorem and contour integration[69], we have

$$\mathbf{c}(t)=\mathbf{Z}(t)+\left[\int_{B_+}\frac{d\omega}{2\pi}+\int_{B_-}\frac{d\omega}{2\pi}\right]\tilde{\mathbf{c}}(-i\omega)e^{-i\omega t}, \tag{18}$$

where $\mathbf{Z}(t)=\sum_{\alpha=\mathrm{bic,boc}}\sum_{j=1}^{N}\mathrm{Res}[\tilde{\mathbf{c}}(-i\omega_j^\alpha)]e^{-i\omega_j^\alpha t}$, with $\mathrm{Res}[\tilde{\mathbf{c}}(-i\omega_j^\alpha)]$ being the residue contributed by the j th bound state obtained from Eq. (17) with eigenenergy $E_j^\alpha=\hbar\omega_j^\alpha$, and the second term comes from the branch cut of the contour. Oscillating with time in continuously changing frequencies, the second term tends to zero in the long-time limit due to the out-of-phase interference. Thus, if the bound state is absent, then $\lim_{t\to\infty}\mathbf{c}(t)=\mathbf{0}$ characterizes a complete relaxation of the atom in the isolated tube, while if the bound states are formed, then $\lim_{t\to\infty}\mathbf{c}(t)=\mathbf{Z}(t)$ implies either a stable distribution or a lossless oscillation of the atom among the optical lattice. Both of the results are absent in the Born-Markovian approximation.

Derivation of the energy spectrum

The eigenstate of Eq. (1) is expanded as $|\Phi\rangle=\sum_{j=1}^{N}x_j|a_j,\{0_k\}\rangle+\sum_k y_k|b,1_k\rangle$. From the eigen equation $\hat{H}|\Phi\rangle=E|\Phi\rangle$, we obtain

$$(E/\hbar-\omega)x_j=\sum_k g_{jk}y_k, \tag{19}$$

$$(E/\hbar-\omega)y_k=\sum_{l=1}^{N}g_{lk}^*x_l. \tag{20}$$

The substitution of the solution of Eq. (20), i.e., $y_k=\sum_{l=1}^{N}g_{lk}^*x_l/(E/\hbar-\omega)$, into Eq. (19) leads to $(E/\hbar-\omega)x_j=-i\sum_{l=1}^{N}f_{jl}(-iE/\hbar)x_l$, which can be tightly rewritten in a matrix form as

$$[E/\hbar-\omega_0+i\tilde{\mathbf{f}}(-iE/\hbar)]\mathbf{x}=0, \tag{21}$$

where $\mathbf{x}=(x_1\cdots x_N)^{\mathrm{T}}$. The Jordan decomposition in Eq. (15) readily converts Eq. (21) into

$$E/\hbar-\omega_0+iD_j(-iE/\hbar)=0, \tag{22}$$

which determines the eigenenergies E of the system.

It is interesting to find that the pole equation (17) determining the tunneling dynamics is just the eigenenergy equation (22) after making the replacement of $E/\hbar=i s$. Just for this reason, we call the eigenstates corresponding to the removable singularities of $D_j(s)$ the BICs and the ones corresponding to the isolated poles the BOCs. This result reveals that the tunneling dynamics of the atom is essentially governed by the feature of the energy spectrum. If neither BOC nor BIC is formed, then $|c_j(t)|$ tends to zero with time and thus the atom eventually relaxes into the tube as a matter wave. If either the BOCs or BICs are formed, then the atom tends to a lossless coherent tunneling among the N lattice sites in multiple frequencies determined by the difference of any pairs of the eigenenergies of the formed BOCs and BICs.

The case of $N=2$

The spectral density matrix for the two lattice sites is $\mathbf{J}(\omega)=\begin{pmatrix}J_0(\omega) & J_1(\omega)\\ J_1(\omega) & J_0(\omega)\end{pmatrix}$. It contributes to the Laplace transform of $\mathbf{f}(t-\tau)$ as $\tilde{\mathbf{f}}(s)=\begin{pmatrix}\tilde{f}_0(s) & \tilde{f}_1(s)\\ \tilde{f}_1(s) & \tilde{f}_0(s)\end{pmatrix}$, where $\tilde{f}_j(s)=\int_0^\infty d\omega\frac{J_j(\omega)}{s+i\omega}$. The Jordan decomposition of $\tilde{\mathbf{f}}(s)$ reads

$$\mathbf{D}(s)=\mathrm{diag}[\tilde{f}_0(s)+\tilde{f}_1(s),\tilde{f}_0(s)-\tilde{f}_1(s)] \tag{23}$$

under $\mathbf{V}_s=\begin{pmatrix}1 & 1\\ 1 & -1\end{pmatrix}$. Thus, we have

$$\tilde{\mathbf{c}}(s)=\begin{pmatrix}1/2 & 1/2\\ 1/2 & -1/2\end{pmatrix}\begin{pmatrix}[s+i\omega_0+D_1(s)]^{-1}\\ [s+i\omega_0+D_2(s)]^{-1}\end{pmatrix}. \tag{24}$$

We need to make the inverse Laplace transform to obtain $\mathbf{c}(t)$. The equations determining the poles of the inverse Laplace transform are

$$Y_1(\varpi)\equiv\omega_0-\int_0^\infty d\omega\frac{J_0(\omega)+J_1(\omega)}{\omega-\varpi}=\varpi, \tag{25}$$

$$Y_2(\varpi)\equiv\omega_0-\int_0^\infty d\omega\frac{J_0(\omega)-J_1(\omega)}{\omega-\varpi}=\varpi, \tag{26}$$

where $\varpi=E/\hbar=i s$. Their solutions can be classified into the following types.

1. In the regime $\varpi>0$, the integration in both $Y_1(\varpi)$ and $Y_2(\varpi)$ is divergent. Thus, they jump rapidly between $\pm\infty$ and Eqs. (25) and (26) have infinite continuous roots, which form an energy band after multiplying $\hbar$ as well as the branch cut.
2. In the regime $\varpi<0$, both $Y_1(\varpi)$ and $Y_2(\varpi)$ are a monotonically decreasing function with ϖ. Thus, one and only one root ϖ_j^{boc} exists for either Eq. (25) or Eq. (26) as long as $Y_j(0)<0$. Since this type of root ϖ_j^{boc} resides in a position out of the continuous energy band, we call it eigenstate BOC.

3. In the regime $\varpi > 0$, the integration in $Y_1(\varpi)$ and $Y_2(\varpi)$ has removable singularities $\varpi_j^{\rm bic}$ determined by $J_0(\varpi_1^{\rm bic}) + J_1(\varpi_1^{\rm bic}) = 0$ and $J_0(\varpi_2^{\rm bic}) - J_1(\varpi_1^{\rm bic}) = 0$ such that Eqs. (25) or (26) is respectively satisfied when $\omega_0 = \varpi_1^{\rm bic} + iD_1(-i\varpi_1^{\rm bic})$ or $\omega_0 = \varpi_2^{\rm bic} + iD_2(-i\varpi_2^{\rm bic})$. We readily evaluate that the removable singularities are $\varpi_{1/2}^{\rm bic} = \tilde{\omega}(\bar{z}n_{1/2}\pi/d)^2/2$, with $d = |z_1 - z_2|$, n_1, and n_2 being odd and even numbers. Since this type of root $\varpi_j^{\rm bic}$ resides in a position in the continuous energy band, we call its corresponding eigenstate BIC.

The residue contributed by the l th bound state with frequency $\bar{\omega}_l^{\alpha}$ evaluated from $Y_l(\varpi) = \varpi$ to the inverse Laplace transform $[s + i\omega_0 + D_j(s)]^{-1}$ in Eq. (24) is

$$\begin{aligned} &\lim_{s\to -i\bar{\omega}_l^{\alpha}}(s + i\bar{\omega}_l^{\alpha})e^{st}[s + i\omega_0 + D_j(s)]^{-1} \\ = \;& Z_l^{\alpha}e^{-i\bar{\omega}_l^{\alpha}t}\delta_{l,j}, \end{aligned} \tag{27}$$

where $Z_l^{\alpha} = [1 + \partial_s D_l(s)]^{-1}|_{s\to -i\bar{\omega}_l^{\alpha}}$. Based on the fact that the steady-state solution of $\mathbf{c}(t)$ obtained via the inverse Laplace transform $\tilde{\mathbf{c}}(s)$ is governed by the residues contributed by the eigenenergies of the BOCs and BICs, we readily have

$$\mathbf{c}(\infty) = \sum_{\alpha={\rm bic,boc}} \begin{pmatrix} 1/2 & 1/2 \\ 1/2 & -1/2 \end{pmatrix} \begin{pmatrix} Z_1^{\alpha}e^{-i\bar{\omega}_1^{\alpha}t} \\ Z_2^{\alpha}e^{-i\bar{\omega}_2^{\alpha}t} \end{pmatrix} \tag{28}$$

in the case of two bound states are formed.

The case of $N = 3$

The spectral density matrix in the case of $N = 3$ reads $\mathbf{J}(\omega) = \begin{pmatrix} J_0(\omega) & J_1(\omega) & J_2(\omega) \\ J_1(\omega) & J_0(\omega) & J_1(\omega) \\ J_2(\omega) & J_1(\omega) & J_0(\omega) \end{pmatrix}$. It contributes to the Laplace transform of $\mathbf{f}(t-\tau)$ as $\tilde{\mathbf{f}}(s) = \begin{pmatrix} \tilde{f}_0 & \tilde{f}_1 & \tilde{f}_2 \\ \tilde{f}_1 & \tilde{f}_0 & \tilde{f}_1 \\ \tilde{f}_2 & \tilde{f}_1 & \tilde{f}_0 \end{pmatrix}$, where the argument "$s$" of $\tilde{f}_j(s)$ has been omitted for brevity. The Jordan decomposition of $\tilde{\mathbf{f}}(s)$ is

$$\mathbf{D}(s) = {\rm diag}[\tilde{f}_0 - \tilde{f}_2, \tilde{f}_0 + \tfrac{1}{2}(\tilde{f}_2 - \tilde{e}), \tilde{f}_0 + \tfrac{1}{2}(\tilde{f}_2 + \tilde{e})] \tag{29}$$

under $\mathbf{V}_s = \begin{pmatrix} -1 & 1 & 1 \\ 0 & \frac{\tilde{f}_1(\tilde{e}-3\tilde{f}_2)}{\tilde{f}_2\tilde{e}-2\tilde{f}_1^2-\tilde{f}_2^2} & \frac{\tilde{f}_1(\tilde{e}+3\tilde{f}_2)}{\tilde{f}_2\tilde{e}+2\tilde{f}_1^2+\tilde{f}_2^2} \\ 1 & 1 & 1 \end{pmatrix}$, where $\tilde{e} = \sqrt{8\tilde{f}_1^2 + \tilde{f}_2^2}$. We thus have $\tilde{\mathbf{c}}(s)$ in the case of $N = 3$ as $\tilde{\mathbf{c}}(s) = \mathbf{M}[s + i\omega_0 + \mathbf{D}(s)]^{-1}\begin{pmatrix} 1 & 1 & 1 \end{pmatrix}^{\rm T}$, where $\mathbf{M} = \begin{pmatrix} 1/2 & \frac{1-\tilde{f}_2/\tilde{e}}{4} & \frac{1+\tilde{f}_2/\tilde{e}}{4} \\ 0 & -\tilde{f}_1/\tilde{e} & \tilde{f}_1/\tilde{e} \\ -1/2 & \frac{1-\tilde{f}_2/\tilde{e}}{4} & \frac{1+\tilde{f}_2/\tilde{e}}{4} \end{pmatrix}$. The poles and the eigenenergies are determined by

$$Y_j(\varpi) \equiv \omega_0 - iD_j(-i\varpi) = \varpi. \tag{30}$$

Being similar to the $N = 2$ case, Eq. (30) has three types of roots, i.e., continuous energy band when $\varpi > 0$, isolated poles $\varpi_j^{\rm boc} < 0$

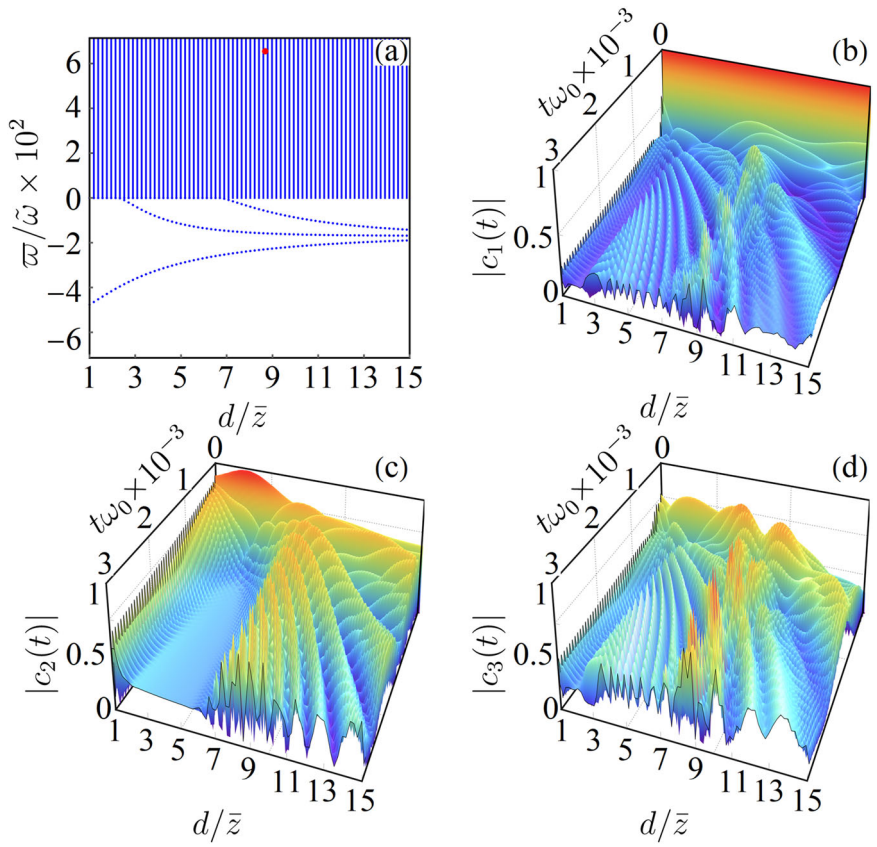

Fig. 6 | Energy spectrum and dynamics for different values of the site separation in the case of three lattice sites. a Energy spectrum for different values of the site separations d. The red point marks the position of the BIC. Evolution of the absolute values of the probability amplitudes (**b**) $|c_1(t)|$, (**c**) $|c_2(t)|$, and (**d**) $|c_3(t)|$. The parameters are $N = 3$, $\Omega = 0.13\tilde{\omega}$, and $\omega_0 = 0.05\tilde{\omega}$.

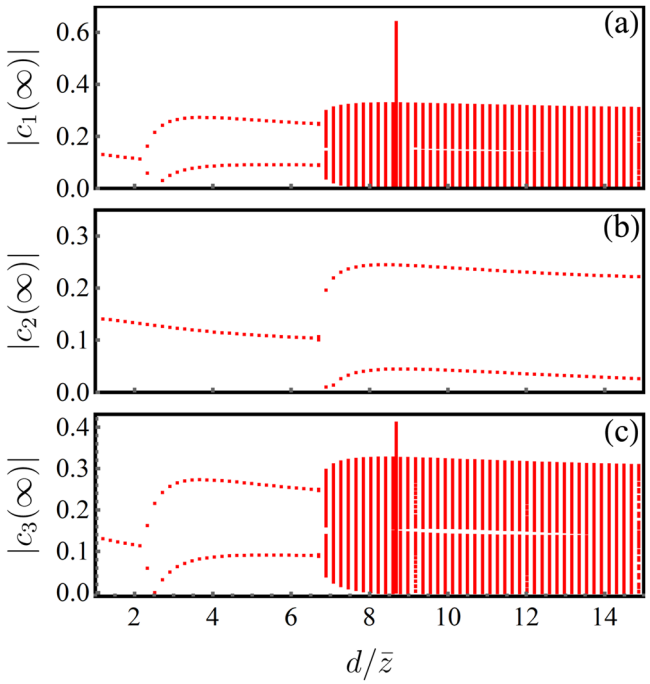

Fig. 7 | Steady-state distribution of the atomic probability amplitudes in the three sites. In the one-BOC regime, (**a**) $|c_1(\infty)|$, (**b**) $|c_2(\infty)|$, and (**c**) $|c_3(\infty)|$ are equal to constants. In the two-BOC regime, (**b**) $|c_2(\infty)|$ keeps being a constant, while $|c_{1/3}(\infty)|$ in **a** and **c** exhibit periodic oscillations in a single frequency, with the maxima and the minima marked by red dots. In the three-BOC regime, (**b**) $|c_2(\infty)|$ exhibits a single-frequency periodic oscillation, with the maxima and the minima marked by red dots, while $|c_{1/3}(\infty)|$ in **a**, **c** exhibit a lossless oscillation in three frequencies, with the local maxima and the minima joined by red lines. The parameters are the same as in Fig. 6.

provided $Y_j(0) < 0$, and discrete removable singularities $\bar{\omega}_j^{\rm bic} > 0$. We can analytically determine that the roots of the BICs for $D_1(s)$ read $\bar{\omega}_1^{\rm bic} = \tilde{\omega}(\bar{z}n\pi/d)^2/8$, with n being an even number, which is formed when $\omega_0 = \bar{\omega}_1^{\rm bic} + iD_1(-i\bar{\omega}_1^{\rm bic})$. Only the BOCs and BICs survive in the long-term dynamics. Thus, according to the residue theorem, we finally obtain

$$c_j(\infty) = \sum_{\alpha={\rm bic,boc}} \sum_{l=1}^{3} \frac{M_{jl}e^{st}}{1+\partial_s D_l(s)}\Big|_{s\to -i\bar{\omega}_l^{\alpha}}. \tag{31}$$

Equation (31) reveals that, in contrast to $c_1(\infty)$ and $c_3(\infty)$, $c_2(\infty)$ does not depend on $\tilde{f}_0(s)$. Therefore, the bound state formed by the $\tilde{f}_0(s)$-branch does not have an impact on $c_2(\infty)$.

The energy spectrum in Fig. 6a reveals that three BOCs and one BIC are formed at most. The evolution of $|c_j(t)|$ in Fig. 6b–d exhibits a one-to-one correspondence to the feature of the energy spectrum. When one BOC is present, the atom tends to a stable probability distribution in the three lattice sites. When two BOCs are present, $|c_{1/3}(t)|$ tends to a periodic oscillation in a frequency equal to the difference of the eigenenergies of the two BOCs divided by $\hbar$, while $|c_2(t)|$ still tends to be a stable value. In this case, the emerged BOC is from $\tilde{f}_0$ and thus has no effect on $|c_2(t)|$. When three BOCs are present, $|c_1(t)|$ and $|c_3(t)|$ tend to an oscillation in three frequencies equal to the differences of the eigenenergies of any pairs of BOCs divided by $\hbar$, while $|c_2(t)|$ tends to a periodic oscillation in one frequency. The analytical results as Eq. (31) are plotted in Fig. 7. The matching of our analytical results with the numerical ones verifies that the long-range tunneling is realized among the three lattice sites as long as multiple BOCs or BICs are present in the energy spectrum.

Data availability

The numerical data for generating the figures are available from authors upon request.

Code availability

The numerical codes for generating the results are also available from authors upon request.

Received: 1 July 2024; Accepted: 20 December 2024;
Published online: 02 January 2025

References

1. Hauge, E. H. & Støvneng, J. A. Tunneling times: a critical review. *Rev. Mod. Phys.* **61**, 917 (1989).
2. Landauer, R. & Martin, T. Barrier interaction time in tunneling. *Rev. Mod. Phys.* **66**, 217 (1994).
3. van der Wiel, W. G. et al. Electron transport through double quantum dots. *Rev. Mod. Phys.* **75**, 1 (2002).
4. Olkhovsky, V. S., Recami, E. & Jakiel, J. Unified time analysis of photon and particle tunnelling. *Phys. Rep.* **398**, 133 (2004).
5. Winful, H. G. Tunneling time, the Hartman effect, and superluminality: a proposed resolution of an old paradox. *Phys. Rep.* **436**, 1 (2006).
6. Ankerhold, J. (eds) *Quantum Tunneling in Complex Systems: The Semiclassical Approach* (Springer Berlin, Heidelberg, 2007). https://doi.org/10.1007/3-540-68076-4
7. Landsman, A. S. & Keller, U. Attosecond science and the tunnelling time problem. *Phys. Rep.* **547**, 1 (2015).
8. Zhu, M. et al. Tunnelling of electrons via the neighboring atom. *Light Sci. Appl.* **13**, 18 (2024).
9. Balantekin, A. B. & Takigawa, N. Quantum tunneling in nuclear fusion. *Rev. Mod. Phys.* **70**, 77 (1998).
10. Hagino, K. & Takigawa, N. Subbarrier fusion reactions and many-particle quantum tunneling. *Prog. Theor. Phys.* **128**, 1061 (2012).
11. Binnig, G., Rohrer, H., Gerber, C. & Weibel, E. Surface studies by scanning tunneling microscopy. *Phys. Rev. Lett.* **49**, 57 (1982).
12. Tersoff, J. & Hamann, D. R. Theory and application for the scanning tunneling microscope. *Phys. Rev. Lett.* **50**, 1998 (1983).
13. Pommier, D. et al. Scanning tunneling microscope-induced excitonic luminescence of a two-dimensional semiconductor. *Phys. Rev. Lett.* **123**, 027402 (2019).
14. Strambini, E. et al. Superconducting spintronic tunnel diode. *Nat. Commun.* **13**, 2431 (2022).
15. Bouscher, S. et al. Enhanced cooper-pair injection into a semiconductor structure by resonant tunneling. *Phys. Rev. Lett.* **128**, 127701 (2022).
16. Löwdin, P.-O. Proton tunneling in DNA and its biological implications. *Rev. Mod. Phys.* **35**, 724 (1963).
17. Cao, J. et al. Quantum biology revisited. *Sci. Adv.* **6**, eaaz4888 (2020).
18. Kim, Y. et al. Quantum biology: an update and perspective. *Quantum Rep.* **3**, 80 (2021).
19. Zuev, P. S. et al. Carbon tunneling from a single quantum state. *Science* **299**, 867 (2003).
20. Wild, R., Nötzold, M., Simpson, M., Tran, T. D. & Wester, R. Tunnelling measured in a very slow ion–molecule reaction. *Nature* **615**, 425 (2023).
21. Suh, D. et al. Electron tunneling of hierarchically structured silver nanosatellite particles for highly conductive healable nanocomposites. *Nat. Commun.* **11**, 2252 (2020).
22. Drechsel-Grau, C. & Marx, D. Quantum simulation of collective proton tunneling in hexagonal ice crystals. *Phys. Rev. Lett.* **112**, 148302 (2014).
23. Borges, H. S., Sanz, L., Villas-Bôas, J. M., Diniz Neto, O. O. & Alcalde, A. M. Tunneling induced transparency and slow light in quantum dot molecules. *Phys. Rev. B* **85**, 115425 (2012).

24. Hamdad, S. et al. Overbias and quantum tunneling in light-emitting memristors. *Phys. Rev. Appl.* **20**, 024057 (2023).
25. Kim, E.-A., Vishveshwara, S. & Fradkin, E. Cooper-pair tunneling in junctions of singlet quantum Hall states and superconductors. *Phys. Rev. Lett.* **93**, 266803 (2004).
26. Reiter, G. F., Mayers, J. & Platzman, P. Direct observation of tunneling in KDP using neutron compton scattering. *Phys. Rev. Lett.* **89**, 135505 (2002).
27. Della Valle, G. et al. Visualization of coherent destruction of tunneling in an optical double well system. *Phys. Rev. Lett.* **98**, 263601 (2007).
28. Lignier, H. et al. Dynamical control of matter-wave tunneling in periodic potentials. *Phys. Rev. Lett.* **99**, 220403 (2007).
29. Kierig, E., Schnorrberger, U., Schietinger, A., Tomkovic, J. & Oberthaler, M. K. Single-particle tunneling in strongly driven double-well potentials. *Phys. Rev. Lett.* **100**, 190405 (2008).
30. Jürgensen, O., Meinert, F., Mark, M. J., Nägerl, H.-C. & Lühmann, D.-S. Observation of density-induced tunneling. *Phys. Rev. Lett.* **113**, 193003 (2014).
31. Liu, W., Zhang, B., Wu, B., Wang, L. & Chen, F. Observation of optical tunneling inhibition by a parabolic potential in twisted photonic lattices. *Phys. Rev. Res.* **4**, L012043 (2022).
32. Fortun, A. et al. Direct tunneling delay time measurement in an optical lattice. *Phys. Rev. Lett.* **117**, 010401 (2016).
33. Fölling, S. et al. Direct observation of second-order atom tunnelling. *Nature* **448**, 1029 (2007).
34. Eckle, P. et al. Attosecond ionization and tunneling delay time measurements in helium. *Science* **322**, 1525 (2008).
35. Sainadh, U. S. et al. Attosecond angular streaking and tunnelling time in atomic hydrogen. *Nature* **568**, 75 (2019).
36. Camus, N. et al. Experimental evidence for quantum tunneling time. *Phys. Rev. Lett.* **119**, 023201 (2017).
37. Ramos, R., Spierings, D., Racicot, I. & Steinberg, A. M. Measurement of the time spent by a tunnelling atom within the barrier region. *Nature* **583**, 529 (2020).
38. Yu, M. et al. Full experimental determination of tunneling time with attosecond-scale streaking method. *Light Sci. Appl.* **11**, 215 (2022).
39. Deng, Y.-H., Lü, H.-F., Ke, S.-S., Guo, Y. & Zhang, H.-W. Quantum tunneling through a rectangular barrier in multi-Weyl semimetals. *Phys. Rev. B* **101**, 085410 (2020).
40. Yu, Q. et al. Highly sensitive strain sensors based on piezotronic tunneling junction. *Nat. Commun.* **13**, 778 (2022).
41. Ma, R. et al. Photon-assisted tunneling in a biased strongly correlated Bose gas. *Phys. Rev. Lett.* **107**, 095301 (2011).
42. Gallego-Marcos, F., Sánchez, R. & Platero, G. Photon assisted long-range tunneling. *J. Appl. Phys.* **117**, 112808 (2015).
43. Braakman, F. R., Barthelemy, P., Reichl, C., Wegscheider, W. & Vandersypen, L. M. K. Long-distance coherent coupling in a quantum dot array. *Nat. Nanotechnol.* **8**, 432 (2013).
44. Winkler, J. R. & Gray, H. B. Long-range electron tunneling. *J. Am. Chem. Soc.* **136**, 2930 (2014).
45. Bueno, P. R. On the fundamentals of quantum rate theory and the long-range electron transport in respiratory chains. *Chem. Soc. Rev.* **53**, 5348 (2024).
46. Meinert, F. et al. Observation of many-body dynamics in long-range tunneling after a quantum quench. *Science* **344**, 1259 (2014).
47. Kessing, R. K., Yang, P.-Y., Manmana, S. R. & Cao, J. Long-range nonequilibrium coherent tunneling induced by fractional vibronic resonances. *J. Phys. Chem. Lett.* **13**, 6831 (2022).
48. Martinez, M. et al. Chaos-assisted long-range tunneling for quantum simulation. *Phys. Rev. Lett.* **126**, 174102 (2021).
49. Krinner, L., Stewart, M., Pazmino, A., Kwon, J. & Schneble, D. Spontaneous emission of matter waves from a tunable open quantum system. *Nature* **559**, 589 (2018).
50. Stewart, M., Kwon, J., Lanuza, A. & Schneble, D. Dynamics of matter-wave quantum emitters in a structured vacuum. *Phys. Rev. Res.* **2**, 043307 (2020).
51. Kwon, J., Kim, Y., Lanuza, A. & Schneble, D. Formation of matter-wave polaritons in an optical lattice. *Nat. Phys.* **18**, 657 (2022).
52. de Vega, I., Porras, D. & Ignacio Cirac, J. Matter-wave emission in optical lattices: Single particle and collective effects. *Phys. Rev. Lett.* **101**, 260404 (2008).
53. Navarrete-Benlloch, C., de Vega, I., Porras, D. & Cirac, J. I. Simulating quantum-optical phenomena with cold atoms in optical lattices. *N. J. Phys.* **13**, 023024 (2011).
54. Stewart, M., Krinner, L., Pazmi no, A. & Schneble, D. Analysis of non-Markovian coupling of a lattice-trapped atom to free space. *Phys. Rev. A* **95**, 013626 (2017).
55. González-Tudela, A., Mu noz, C. S. & Cirac, J. I. Engineering and harnessing giant atoms in high-dimensional baths: a proposal for implementation with cold atoms. *Phys. Rev. Lett.* **122**, 203603 (2019).
56. González-Tudela, A. & Cirac, J. I. Non-Markovian quantum optics with three-dimensional state-dependent optical lattices. *Quantum* **2**, 97 (2018).
57. Bello, M., Platero, G., Cirac, J. I. & González-Tudela, A. Unconventional quantum optics in topological waveguide qed. *Sci. Adv.* **5**, eaaw0297 (2019).
58. Bloch, I., Dalibard, J. & Zwerger, W. Many-body physics with ultracold gases. *Rev. Mod. Phys.* **80**, 885 (2008).
59. Lanuza, A., Kwon, J., Kim, Y. & Schneble, D. Multiband and array effects in matter-wave-based waveguide QED. *Phys. Rev. A* **105**, 023703 (2022).
60. Tavis, M. & Cummings, F. W. Exact solution for an *n*-molecule—radiation-field Hamiltonian. *Phys. Rev.* **170**, 379 (1968).
61. Davies, E. B. Markovian master equations. *Commun. Math. Phys.* **39**, 91 (1974).
62. Dümcke, R. & Spohn, H. The proper form of the generator in the weak coupling limit. *Z. f.ür. Phys. B Condens. Matter* **34**, 419 (1979).
63. Shahmoon, E. & Kurizki, G. Nonradiative interaction and entanglement between distant atoms. *Phys. Rev. A* **87**, 033831 (2013).
64. Yang, C.-J., An, J.-H. & Lin, H.-Q. Signatures of quantized coupling between quantum emitters and localized surface plasmons. *Phys. Rev. Res.* **1**, 023027 (2019).
65. Wu, W. & An, J.-H. Gaussian quantum metrology in a dissipative environment. *Phys. Rev. A* **104**, 042609 (2021).
66. Zhang, N., Chen, C., Bai, S.-Y., Wu, W. & An, J.-H. Non-Markovian quantum thermometry. *Phys. Rev. Appl.* **17**, 034073 (2022).
67. Wu, W. & An, J.-H. Quantum speed limit of a noisy continuous-variable system. *Phys. Rev. A* **106**, 062438 (2022).
68. Ji, F.-Z., Bai, S.-Y. & An, J.-H. Strong coupling of quantum emitters and the exciton polariton in MoS_2 nanodisks. *Phys. Rev. B* **106**, 115427 (2022).
69. Wu, W., Bai, S.-Y. & An, J.-H. Non-Markovian sensing of a quantum reservoir. *Phys. Rev. A* **103**, L010601 (2021).
70. Sheremet, A. S., Petrov, M. I., Iorsh, I. V., Poshakinskiy, A. V. & Poddubny, A. N. Waveguide quantum electrodynamics: collective radiance and photon-photon correlations. *Rev. Mod. Phys.* **95**, 015002 (2023).
71. Awschalom, D. et al. Development of quantum interconnects (QuICs) for next-generation information technologies. *PRX Quantum* **2**, 017002 (2021).
72. Lonigro, D. The self-energy of friedrichs-lee models and its application to bound states and resonances. *Eur. Phys. J.* **137**, 492 (2022).
73. Gross, C. & Bloch, I. Quantum simulations with ultracold atoms in optical lattices. *Science* **357**, 995 (2017).
74. Yngvesson, S. Tunneling devices. In *Microwave Semiconductor Devices* 103–126 (Springer US, Boston, 1991). https://doi.org/10.1007/978-1-4615-3970-4_4.

75. Niu, J. et al. Low-loss interconnects for modular superconducting quantum processors. *Nat. Electron.* **6**, 235 (2023).
76. Lei, M. et al. Many-body cavity quantum electrodynamics with driven inhomogeneous emitters. *Nature* **617**, 271 (2023).
77. Mirhosseini, M. et al. Cavity quantum electrodynamics with atom-like mirrors. *Nature* **569**, 692 (2019).
78. Blais, A., Girvin, S. M. & Oliver, W. D. Quantum information processing and quantum optics with circuit quantum electrodynamics. *Nat. Phys.* **16**, 247 (2020).
79. Blais, A., Grimsmo, A. L., Girvin, S. M. & Wallraff, A. Circuit quantum electrodynamics. *Rev. Mod. Phys.* **93**, 025005 (2021).
80. Song, W.-L., Liu, H.-B., Zhou, B., Yang, W.-L. & An, J.-H. Remote charging and degradation suppression for the quantum battery. *Phys. Rev. Lett.* **132**, 090401 (2024).
81. Bai, S.-Y. & An, J.-H. Generating stable spin squeezing by squeezed-reservoir engineering. *Phys. Rev. Lett.* **127**, 083602 (2021).

Acknowledgements

The work is supported by the National Natural Science Foundation of China (grants no. 12275109, no. 12205128, and no. 12247101) and the Innovation Program for Quantum Science and Technology of China (grant no. 2023ZD0300904).

Author contributions

Jun-Hong An proposed the original idea and developed the theoretical formalism. Yuan-Xing Yang and Si-Yuan Bai performed the analytic derivations. Yuan-Xing Yang drafted the manuscript and designed the figures. All authors discussed the results and contributed to the final manuscript.

Competing interests

The authors declare no competing interests.

Additional information

Correspondence and requests for materials should be addressed to Jun-Hong An.

Peer review information *Communications Physics* thanks András Vukics and the other, anonymous, reviewer(s) for their contribution to the peer review of this work.